The Indian Ocean Dipole: A Monopole in SST

YONGJING ZHAO AND SUMANT NIGAM

Department of Atmospheric and Oceanic Science, University of Maryland, College Park, College Park, Maryland

(Manuscript received 14 January 2014, in final form 13 May 2014)

ABSTRACT

The claim for a zonal-dipole structure in interannual variations of the tropical Indian Ocean (IO) SSTs—the Indian Ocean dipole (IOD)—is reexamined after accounting for El Niño–Southern Oscillation's (ENSO) influence. The authors seek an a priori accounting of ENSO's seasonally stratified influence on IO SSTs and evaluate the basis of the related dipole mode index, instead of seeking a posteriori adjustments to this index, as common.

Scant observational evidence is found for zonal-dipole SST variations after removal of ENSO's influence from IO SSTs: The IOD poles are essentially uncorrelated in the ENSO-filtered SSTs in both recent (1958–98) and century-long (1900–2007) periods, leading to the breakdown of zonal-dipole structure in *surface* temperature variability; this finding does not depend on the subtleties in estimation of ENSO's influence. Deconstruction of the fall 1994 and 1997 SST anomalies led to their reclassification, with a weak IOD in 1994 and none in 1997.

Regressions of the eastern IOD pole on upper-ocean heat content, however, do exhibit a zonal-dipole structure but with the western pole in the central-equatorial IO, suggesting that internally generated basin variability can have zonal-dipole structure at the *subsurface*.

The IO SST variability was analyzed using the extended-EOF technique, after removing the influence of Pacific SSTs; the technique targets spatial *and* temporal recurrence and extracts modes (rather than patterns) of variability. This spatiotemporal analysis also does not support the existence of zonal-dipole variability at the surface. However, the analysis did yield a dipole-like structure in the meridional direction in boreal fall/winter, when it resembles the subtropical IOD pattern (but not the evolution time scale).

1. Introduction

The tropical Indian Ocean (IO) basin—home to pronounced seasonal low-level wind variability including direction reversal (monsoonal flow)—exhibits notably weak interannual variability in SST and surface winds (e.g., Nigam and Shen 1993), especially in comparison with the Pacific where interannual El Niño–Southern Oscillation (ENSO) variability is impressive and influential. The proximity of the two basins and ENSO's large-scale structure and near-global response provides scope for basin interaction. ENSO, in fact, does influence the Indian Ocean SST and low-level winds, especially during July–November (Nigam and Shen 1993, see their Fig. 2).

More recently, Saji et al. (1999) identified a dipole pattern of SST variability in the tropical Indian Ocean, which is widely referred to as the Indian Ocean dipole (IOD). The identification was based on the EOF analysis of SST anomalies of all calendar months in the 1958–98 period. The leading pattern, describing basin-scale anomalies of uniform polarity, was taken to represent the ENSO influence on the Indian Ocean, and the second pattern, the IOD, was thus considered temporally independent of ENSO. This basic premise of Saji et al. is questioned in this study.

Saji et al.'s characterization of their leading EOF pattern as representing ENSO's influence on the Indian Ocean is reexamined for the following reasons. First, ENSO's influence varies with season whereas their leading EOF is seasonally invariant: The ENSO-related warming of the tropical Indian Ocean, for example, is focused in the northwestern basin in summer and fall and in its southeastern sector in boreal winter (Nigam and Shen 1993, their Figs. 2 and 4). Second, characterizing (filtering) ENSO's influence is challenging as its

Corresponding author address: Sumant Nigam, Department of Atmospheric and Oceanic Science, 3419 Computer and Space Science Building, University of Maryland, College Park, College Park, MD 20742-2425.
E-mail: nigam@umd.edu

DOI: 10.1175/JCLI-D-14-00047.1

evolution is not representable by a single index or EOF due to complex spatiotemporal development (e.g., Guan and Nigam 2008, hereafter GN2008; Compo and Sardeshmukh 2010). Saji et al.'s characterization of the leading EOFs thus requires reconsideration.

Since Saji et al.'s analysis, the IOD structure and impacts have been widely analyzed using the dipole mode index (DMI; Saji et al. 1999). The DMI index, interestingly, is neither tightly correlated with the second EOF's time series (~0.7, or only 50% common variance) nor independent of ENSO (correlation with Niño-3.0 SST index is ~0.35), all as reported in Saji et al. (1999). The correlation of the EOF time series itself with the Niño-3.0 (or related) SST index was not reported by the authors, leaving open the question of IOD's independence from ENSO.

Not surprisingly, the IOD–ENSO link has been extensively debated. Several observational studies lend support to IOD's independence from ENSO (e.g., Behera et al. 1999; Webster et al. 1999; Murtugudde et al. 2000; Ashok et al. 2003; Behera et al. 2003; Yamagata et al. 2003), while others question the same (e.g., Chambers et al. 1999; Reason et al. 2000; Allan et al. 2001; Nicholls and Drosdowsky 2001; Baquero-Bernal et al. 2002; Dommenget and Latif 2002; Hastenrath 2002; Xie et al. 2002; Dommenget 2007; Jansen et al. 2009; Dommenget 2011). Allan et al. (2001) claim that ENSO's spatiotemporal evolution is aliased in the DMI index but these authors did not question the basis of the index itself. Meyers et al. (2007) could not infer a clear link between IOD and ENSO events, attributing the lack of clarity to the decadal variations in thermocline depth off Java and Sumatra.

Modeling studies (e.g., Baquero-Bernal et al. 2002; Shinoda et al. 2004; Yu and Lau 2005; Kug and Kang 2006; Jansen et al. 2009) also provide insights into the contribution of ENSO and ocean dynamics in generating Indian Ocean SST variability. From analysis of the tropical Indian Ocean response to observed wind forcing, Shinoda et al. found the dipole mode to be the leading mode of thermocline depth variability, with the ENSO-independent dipole variability more strongly expressed in the upper-ocean heat content than SSTs. The successive IOD events of 2006 (an El Niño year) and 2007 (a La Niña year) spurred further interest in IOD genesis and predictability (e.g., Luo et al. 2008), including the possibility of IOD's link with noncanonical ENSO variability (Ashok et al. 2007; Luo et al. 2010); the latter is referred to as the noncanonical ENSO mode by GN2008 and El Niño Modoki by Ashok et al. (2007). The evidence for ENSO's influence on the IOD is growing: Yamagata et al. (2004) found one-third of IOD events to be connected with ENSO using seasonally stratified correlations. Behera et al. (2006) found a significant fraction of IOD events correlated with tropical Pacific variability, including ENSO, in their modeling study. The influence of IOD on ENSO has also been investigated (e.g., Wu and Kirtman 2004; Dommenget et al. 2006; Jansen et al. 2009; Izumo et al. 2010; Frauen and Dommenget 2012), with indications of interbasin interaction on both interannual and decadal time scales (Huang and Shukla 2007a,b; Dommenget 2011).

Given the large body of literature on analysis of the IOD–ENSO link, it is, perhaps, necessary to articulate the goals of this observational study:

- Most observational investigations of the IOD–ENSO link begin with IOD's putative characterization—a zonal dipole structure—manifest in the DMI index, and seek index refinement by factoring for ENSO's influence; that is, they seek a posteriori adjustments. This study, in contrast, questions the IOD's canonical characterization itself (i.e., the basis for the DMI index). It thus seeks an a priori accounting of ENSO's influence, like Meyers et al. (2007).
- ENSO's influence on Indian Ocean SSTs is characterized taking into account ENSO's complex development: the spatiotemporally varying impact of both canonical and noncanonical ENSO variability is estimated and filtered *prior* to the search for recurrent modes of SST variability in the Indian Ocean. Many previous studies have estimated this influence—incompletely, in our opinion—from the tracking of ENSO's mature phase alone and related compositing (e.g., Yamagata et al. 2004).
- ENSO-filtered Indian Ocean SSTs are analyzed using the extended empirical orthogonal function technique (extended EOF), which focuses on spatial *and* temporal recurrence and, as such, yields modes (rather than patterns) of variability—all rooted in the Indian Ocean basin, in this case. Unlike some earlier studies (e.g., Behera et al. 2003), SSTs are not smoothed or filtered in any manner, except for ENSO variability, avoiding potential aliasing of the SST record. A century-long SST record is also analyzed here in the interest of robust findings.

The ENSO characterization and the follow-on Indian Ocean SST analysis are based on the recent innovative analysis of natural variability and secular trend in the Pacific (and Atlantic) SSTs in the twentieth century (GN2008). By focusing on spatial *and* temporal recurrence, the extended-EOF analysis discriminates between interannual and decadal-multidecadal variability, and the nonstationary secular trend—all without any advance filtering (and potential aliasing) of the SST record. The Atlantic SSTs were similarly analyzed but after excluding the influence of Pacific SSTs and the SST secular trend on the Atlantic basin (Guan and Nigam

2009), leading to a clarified view of the Atlantic multidecadal oscillation (AMO) structure and the implicit decadal time-scale exchanges of sub-Arctic and North Atlantic water (e.g., the 1980s Great Salinity Anomaly; Guan and Nigam 2009). The Atlantic basin analysis serves as a prototype for this Indian Ocean SST analysis.

The claim for the dipole structure of interannual SST variability in the tropical Indian Ocean is examined in section 3. Section 4 examines if the 1994 and 1997 SST anomalies indeed represent IOD events, as suggested by Saji et al. (1999, their Fig. 1). The search for dipole variability is extended to the Indian Ocean subsurface in section 5, which examines the structure of upper-ocean heat content variations linked with the eastern pole of the IOD (the more viable of the two poles). The IO SST analysis is described in section 6 and concluding remarks follow in section 7.

2. Datasets

The UK Met Office's Hadley Centre Sea Ice and Sea Surface Temperature dataset (HadISST 1.1; Rayner et al. 2003) is analyzed in both the Saji et al. analysis period (1958–98) and the century-long period (1900–2007) in section 3. The extended EOF analysis of filtered Indian Ocean SSTs in the period 1900–2007 is discussed in section 6. The linear regressions reported in sections 4 and 6 are computed for the 1902–2005 period, given the end-point truncation of the principal components (PCs) in extended-EOF analysis.

The Simple Ocean Data Assimilation (SODA) 2.1.6 dataset is used for computing the upper-ocean heat content (Carton et al. 2000; Carton and Giese 2008). The SODA heat content (0–381 m) analysis is confined to 1958–98, the common period of the Saji et al. analysis, 1958–98, and the 40-yr European Centre for Medium-Range Weather Forecasts (ECMWF) Re-Analysis (ERA-40; Uppala et al. 2005), 1958–2001. The SODA 2.1.6 ocean reanalysis is, interestingly, driven by the ERA-40 winds, which are also analyzed here. The Climate Research Unit TS 3.1 (CRU TS3.1) dataset is used in the continental precipitation analysis reported in section 6. All datasets are analyzed at seasonal resolution.

3. Variability in ENSO-filtered Indian Ocean SSTs: No evidence for a zonal dipole

The claim for a dipole structure of interannual variability in tropical Indian Ocean SSTs rests on the zonal structure of the second-leading EOF in Saji et al. (1999)—a dipole structure—that led to the DMI index. The index is from the difference of area-averaged SST anomalies in the western (10°S–10°N, 50°–70°E) and eastern (10°S–0°, 90°–108°E) tropical Indian Ocean; the regions are marked in black in Fig. 1. Although these regions are identified from a dipole-type EOF structure, there is no assurance that they are anticorrelated as EOFs often pick up structure to maximize explained variance (e.g., Dommenget and Latif 2002).

The connectedness of the western and eastern Indian Ocean regions—the two poles of the claimed dipole—is investigated in boreal fall in Fig. 1. The Saji et al. period (1958–98) is analyzed first using the detrended SST anomaly record.[1] Regressions of the western IOD box (the W-IOD box; 10°S–10°N, 50°–70°E) (Fig. 1a) support the dipole nature of variability but with a slightly southeastward displaced eastern center vis-à-vis IOD's eastern box. Regressions of the eastern box (the E-IOD box; 10°S–0°, 90°–108°E), shown in Fig. 1b are, however, focused in the south-central equatorial IO rather than the western box, diminishing reciprocity between the marked dipole centers. Support for the western box as a center of action of the dipole is even less in the century-long analysis (Fig. 1f) which exhibits vanishing regressions over this region.

The connectedness of the IOD centers crumbles upon removal of the ENSO signal from the IO SSTs, irrespective of the analysis period. The spatiotemporally varying ENSO influence was estimated by multiplying the time-dependent Pacific SST PCs of canonical ENSO variability [captured as two modes, the growth ($ENSO^-$) and decay ($ENSO^+$) modes in GN2008 (see their Fig. 3)], noncanonical ENSO variability ($ENSO^{NC}$ in GN2008, their Fig. 5), and biennial variability (GN2008, their Fig. 10) with their respective regressions on contemporaneous IO SSTs in the full record (1900–2007).[2] The Indian Ocean SSTs, filtered for this ENSO

[1] The century-long (1900–2007) anomaly record was detrended by subtracting the projections of the SST secular trend mode (GN2008, their Fig. 13 and related discussion) from the seasonal anomalies. A *linearly* detrended SST anomaly record could just as well be used. A subperiod (1958–98) of the detrended record is analyzed in the left panels while the full record (1900–2007) is analyzed in the right ones of Fig. 1.

[2] ENSO is taken to consist of canonical, noncanonical, and biennial variability, consistent with prevailing views. For example, Rasmusson et al. (1990) viewed ENSO as superposition of biennial and lower-frequency variability; see Fig. 8 in GN2008 for the impact of biennial variability on ENSO duration. That biennial variability is an integral component of ENSO is also indicated by correlations of the observed Niño-3.4 SST index and its synthetic versions based on various SST reconstructions. For example, if only canonical ENSO modes are used in SST reconstruction, the correlation is 0.84; correlation increases to 0.92 when the noncanonical ENSO mode is additionally included in the reconstruction, and even further to 0.95 when the biennial mode is included as well. The SST principal components are available online at http://dsrs.atmos.umd.edu/DATA/sst_pcs/.

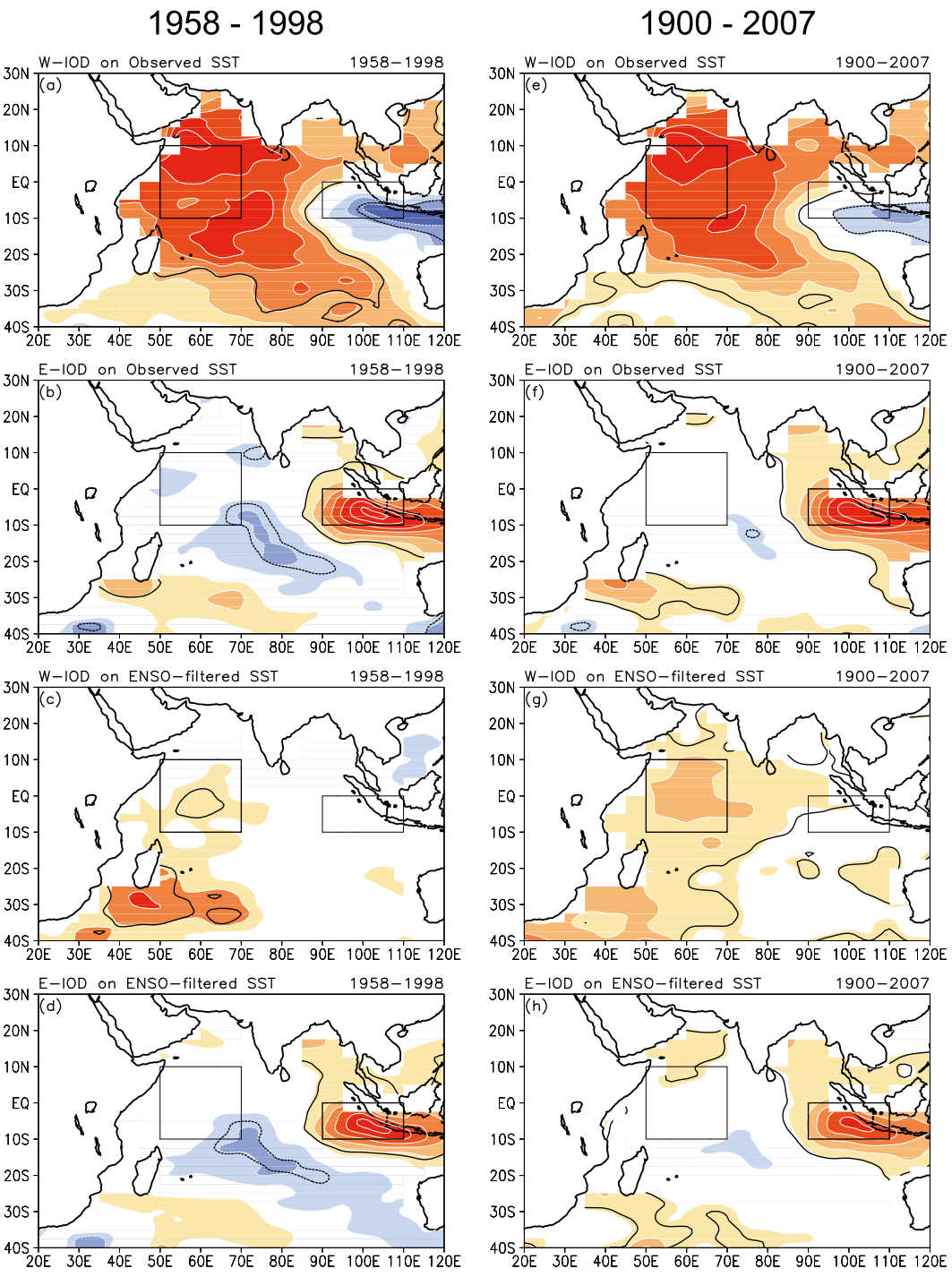

FIG. 1. Evaluation of the basis for Indian Ocean dipole (IOD) mode of SST variability from both recent (1958–98) and century-long (1900–2007) SST records; the former period is identical to that analyzed by Saji et al. (1999). (a) Boreal fall SST regressions of the western-IOD box (W-IOD, marked) based SST index. (b) As in (a), but for the eastern-IOD box (E-IOD, marked) index. Note that the dipole mode index (DMI; Saji et al.) is obtained by subtracting the E-IOD index from the W-IOD one. (c),(d) Fall regressions of the W-IOD and E-IOD indices on ENSO-filtered SSTs; ENSO-filtered SSTs are generated, as noted in the text, by removing the *spatiotemporally evolving* ENSO influence. Corresponding regressions for the century-long period are shown in the right column. In all cases, regressions are computed on detrended SST (following footnote 1). Contour interval and shading threshold is 0.05 K, and positive values are shown in warm colors; the zero contour is omitted in all panels. Regressions significant at the 0.05 level are contoured in black.

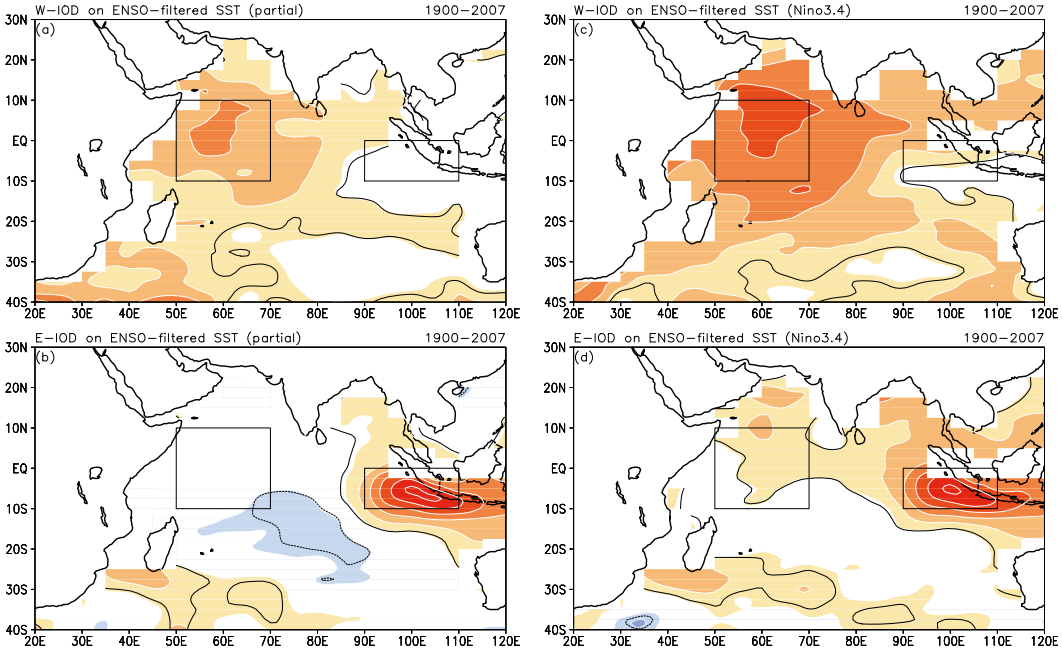

FIG. 2. Two additional constructs of ENSO variability are filtered from Indian Ocean SSTs prior to computation of the regressions of the W-IOD and E-IOD based SST indices: ENSO variability is constructed from (left) the canonical and noncanonical ENSO components only (i.e., without contribution from Pacific biennial variability) and (right) the widely used index of ENSO's mature-phase variability (Niño-3.4 SST index). Boreal fall regressions are for the century-long period (1900–2007); rest as in Fig. 1. Regressions significant at the 0.05 level are contoured in black.

influence, are referred to as filtered SSTs. The analysis of filtered SSTs in the Saji et al. period (1958–98) shows the western dipole center to be nonviable: regressions of the western IOD box have no footprint whatsoever over the eastern box (Fig. 1c), and likewise for regressions of the eastern IOD box (Fig. 1d) over the other region. The eastern box is again found more connected to the south-central equatorial IO SSTs,[3] albeit more weakly than before. The century-long (1900–2007) analysis of filtered SSTs (Figs. 1g,h) corroborates the shorter-period findings, as does an inspection of the related correlation maps (not shown).

Given the premium placed on characterization of ENSO's influence on IO SSTs, it is, perhaps, essential to evaluate the sensitivity of our findings to different estimations of this influence. Two estimates are considered in Fig. 2 where the fall-season connectivity of IOD centers is investigated in the century-long period (1900–2007). The first is based on canonical and noncanonical ENSO components alone (i.e., without additional contribution from Pacific biennial variability, as in Fig. 1); this is referred to as ENSO-filtered (partial). A comparison of Figs. 1g and 2a, and of Figs. 1h and 2b, shows the continued nonviability of either of the IOD centers. The second estimate is based on the widely used index of ENSO's mature-phase variability, the Niño-3.4 SST index. Although ENSO's influence is commonly estimated in this manner, the estimation is suboptimal for reasons stated earlier (and in Compo and Sardeshmukh 2010). Regardless, its filtering does not lead to the emergence of any support for opposite-signed connectivity of the IOD centers (Figs. 2c,d).

We find that ENSO-filtered Indian Ocean SSTs do not exhibit a zonal-dipole variability structure with centers of action as defined in Saji et al. (1999). The analysis of *surface* temperature does not support the DMI concept, which was shown to result from the inadvertent inclusion of ENSO's spatiotemporal influence on Indian Ocean SSTs in the Saji et al. analysis.

The search for a zonal-dipole variability structure in the tropical Indian Ocean is extended into the *subsurface* realm in section 5, from analysis of the upper-ocean heat content variations. The search is rooted in regressions of the eastern pole of the IOD (E-IOD), which is a center of robust dynamical variability on account of regional ocean–atmosphere interaction including upwelling off Java and Sumatra. Meyers et al. (2007) and Luo et al. (2010) have used the E-IOD index to characterize the internal mode of IO variability.

[3] The south-central equatorial IO region cannot be a viable western dipole center given the vanishing regressions of the eastern center in this region in the longer period analysis (Fig. 1h).

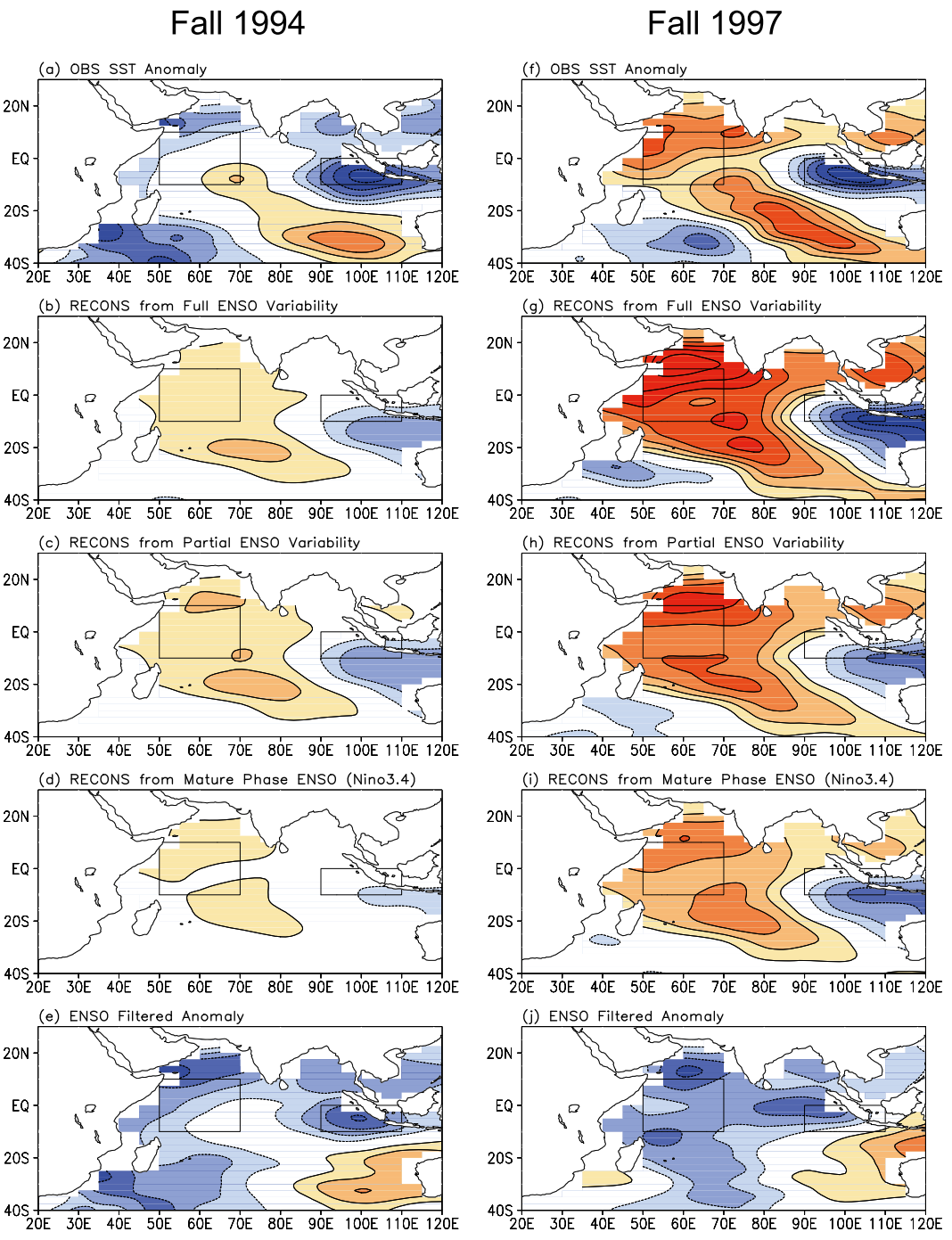

FIG. 3. (a)–(j) Origin of the fall 1994 and 1997 Indian Ocean SST anomalies: (top) observed anomalies; (second row) anomalies reconstructed from ENSO's *full* influence (canonical, noncanonical, biennial modes); (third row) those reconstructed from ENSO's *partial* influence (canonical, noncanonical modes; (fourth row) those reconstructed using ENSO's mature-phase index (Niño-3.4 SST index); and (bottom) fully ENSO-filtered anomalies. Detrended SSTs are the starting point in all cases. The western and eastern IOD box is displayed in all panels to facilitate IOD recognition. Contour interval and shading threshold is 0.15K, and positive values are shown in warm colors; the zero-contour is omitted in all panels. Also shown is the origin of the fall 1994 and 1997 Indian Ocean upper-ocean (0–381 m) heat content anomalies and 850-hPa winds: (k),(m) the ocean heat content anomalies from SODA 2.1.6 reanalysis (Carton et al. 2000) and wind anomalies from ERA-40 atmospheric reanalysis (Uppala et al. 2005), and (l),(n) the fully ENSO-filtered ocean heat content and wind anomalies. The anomalies are displayed after four applications of the 9-point smoother (smth9 in GrADS) with a shading threshold/interval of 2×10^8 J m^{-2}; see color bar; the wind vector scale is shown. Detrended ocean heat content and winds are the starting point in all cases. The western and eastern IOD box is displayed in all panels to facilitate IOD recognition.

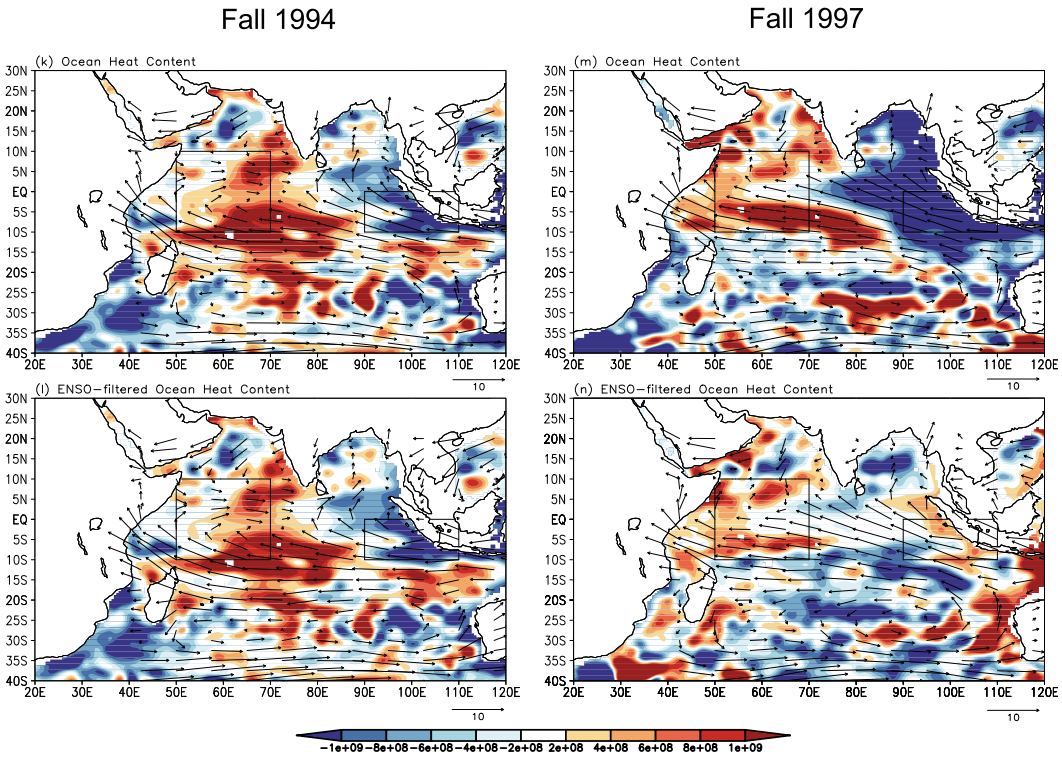

FIG. 3. (*Continued*)

4. The 1994 and 1997 fall SST anomalies: IOD events?

The dipole mode index is strongly positive in the fall of 1994 and 1997 (Saji et al.1999, their Fig. 1); 1994 was a weak El Niño year but the 1997 winter saw one of the strongest warm events on record (NOAA Climate Diagnostic Bulletin). As ENSO's influence is aliased in the DMI definition (cf. Figs. 1 and 2 and related discussion), it is instructive to examine the structure of both raw and ENSO-filtered Indian Ocean SST and upper-ocean (0–381 m) heat content anomalies in these two years; the detrended SSTs and ocean heat content anomalies are the starting point in both cases. SST anomalies are based on the century-long (1900–2007) seasonal climatology, and reconstructed from PCs obtained from an extended-EOF analysis of SSTs in the same period. The ocean heat content anomalies are, of necessity, based on the shorter 41-yr period (1958–98)—the SODA data period, which is also Saji et al.'s analysis period. The SST anomalies are displayed in Figs. 3a–j, while the heat content ones are shown in Figs. 3k–n.

The fall 1994 SST anomaly (top panel) is strongly negative off Sumatra (i.e., over the E-IOD box) but weaker and of mixed sign over the W-IOD box. The DMI is, interestingly, positive [0.60 = (−0.03) − (−0.63)] with similar-signed anomalies in the two IOD boxes. The next three panels display various estimates of ENSO's contribution to the fall 1994 SST anomaly. The one obtained from accounting of the spatiotemporal influence of canonical and noncanonical ENSO variability, and biennial variability (i.e., the full ENSO influence) on IO SSTs is shown in Fig. 3b, while the version without the biennial component is in Fig. 3c. The IO SST anomaly constructed from regressions of the Niño-3.4 SST index is shown in Fig. 3d. All three estimates of ENSO's influence on IO SSTs exhibit a zonal-dipole structure, one that would, undoubtedly, project on the DMI index. The ENSO-*un*related IO SST anomaly (i.e., observed minus ENSO's full influence) is shown in the bottom panel. The SST anomalies off Sumatra are not as strong as before (Fig. 3a) while the ones along the Somali coast and Arabian Sea are stronger (and of the same sign as the Sumatra ones) in the ENSO-filtered version (Fig. 3e), yielding a smaller DMI (0.25) than the one calculated from unfiltered anomalies (Fig. 3a; 0.60).

The fall 1997 SST anomalies are analyzed in the right column of Fig. 3. All three estimates of the ENSO contribution to IO SSTs are now stronger; not surprising, given the unusually strong 1997 El Niño. The large-scale anomaly structure (zonal dipole) is very similar (except for the amplitude) to that seen in the 1994

contributions (Figs. 3b–d), and also among themselves (Figs. 3g–i). The ENSO-filtered IO SST anomaly in 1997 (Fig. 3j), interestingly, does not exhibit an impressive zonal-dipole structure in the IO. The DMI index from the original (Fig. 3f) and ENSO-filtered SST anomalies (Fig. 3j) is 1.05 and −0.09, respectively.

A full accounting of ENSO's contribution to the Indian Ocean surface (SST) anomalies in fall 1994 and 1997 suggests a weak IOD event in 1994, and none at all in 1997. The accounting leads to a rather different assessment in 1997, which was marked as a strongly positive IOD year in previous analyses (e.g., Saji et al. 1999), based on DMI computation off raw SST anomalies.

An IOD event was also reported in fall 2006 (Horii et al. 2008), with a DMI index (0.57) similar to that in fall 1994 (both are weak El Niño years). Reconstruction of the IO SST anomalies indicates a strong ENSO contribution whose filtering leads to a DMI index of 0.14, or a weak IOD event, much as in fall 1994.

Subsurface anomaly structure

In view of the above-noted disagreement in characterization of the nature and structure of the IO SST anomalies in fall of 1994, and especially 1997, the related subsurface anomaly structure is examined in Figs. 3k–n though plots of the upper-ocean heat content; as before, both observed and ENSO-filtered versions are shown. Interestingly, the ENSO-filtered anomaly is nearly indistinguishable from the original one in 1994, but very distinct in 1997 (a strong El Niño year). A zonal-dipole structure is evident in 1994 but with the western pole located to the right of the W-IOD box, but no dipole structure is manifest in the filtered 1997 heat-content anomaly (Fig. 3n). Strong southeasterlies are present on the west coast of Sumatra in both cases (Figs. 3k,m), leading to coastal upwelling and colder SSTs. The ENSO-filtered winds (Figs. 3l,n) remain southeasterly but the filtered SSTs off Sumatra are cold only in fall 1994, indicating the significance of other influences on SST in fall 1997. The similarity of the observed and ENSO-filtered winds attests to the rather modest influence of ENSO on Indian Ocean winds ($\sim$1–2 m s^{-1}), consistent with earlier diagnoses of this signal (e.g., Nigam and Shen 1993, see their Fig. 2). The fall 2006 anomalies (not shown) are similar to the 1994 ones in that their ENSO-filtered versions exhibit weak IOD variability in SST but robust dipole variability in subsurface temperatures.

This limited analysis (two cases) suggests that the tropical IO basin can exhibit internally generated zonal-dipole structure, but mainly at the subsurface. Externally driven IO variability (e.g., from ENSO's influence), on the other hand, can generate zonal-dipole type structure both at the surface and subsurface. If this analysis is corroborated from additional observational and modeling studies, it would caution against identification of IOD events from surface analysis.

5. Seasonally evolving subsurface variability in the Indian Ocean: ENSO's influence

The upper-ocean (0–381 m) heat content is an integrated measure of ocean temperature, reflecting input from surface fluxes, advective transports, and upwelling; it is thus a more steady measure of the upper-ocean state than SST (Merle 1980). Positive/negative ocean heat content (OHC) anomalies are generally indicative of positive (negative) subsurface temperature anomalies, a deepening (shoaling) thermocline, and at times, anomalously high (low) SSTs.

The seasonal evolution of OHC and 850-hPa wind anomalies associated with fall SST variability at the E-IOD box—the more viable dipole center—is displayed in Fig. 4; the 850-hPa winds, and not surface winds, are displayed to preclude use of extrapolated winds over adjoining landmasses. Regressions of three versions of the E-IOD SST index are shown: lead/lag regressions of the "raw" (i.e., unfiltered) index are in the top row, of an index constructed from just ENSO related IO variability in the middle, and of the ENSO-filtered E-IOD index are in the bottom row. Seasonal anomalies are analyzed: The summer [June–August (JJA)] anomalies (first column) are the one-season lead regressions while the winter [December–February (DJF)] ones (last column) are the one-season lag regressions; contemporaneous [fall; i.e., September–November (SON)] ones are in the middle column.

Regressions of the E-IOD will naturally bring out the negative phase IOD structure, when temperatures and OHC off Sumatra are above normal, and strong westerly anomalies blow across the western coast of Sumatra (Fig. 4b); the alongshore winds being from the northwest lead to coastal downwelling. Equatorial westerlies, on the other hand, generate downwelling over the open ocean, leading to thermocline depression over the eastern equatorial basin. Downwelling equatorial and coastally trapped Kelvin waves also contribute to the positive OHC anomalies in this region (Wyrtki 1973; Clarke and Liu 1993). The southwesterly anomalies across the southwestern equatorial IO basin generate upwelling Rossby waves, leading to shallower thermocline and negative OHC anomalies here (Fig. 4b; Meehl et al. 2003); related regional feedbacks have also been proposed (e.g., Saji et al. 1999). The off-shore westerly anomalies (and related moisture transports), evident especially off Somalia in Fig. 4b, have, of course, been

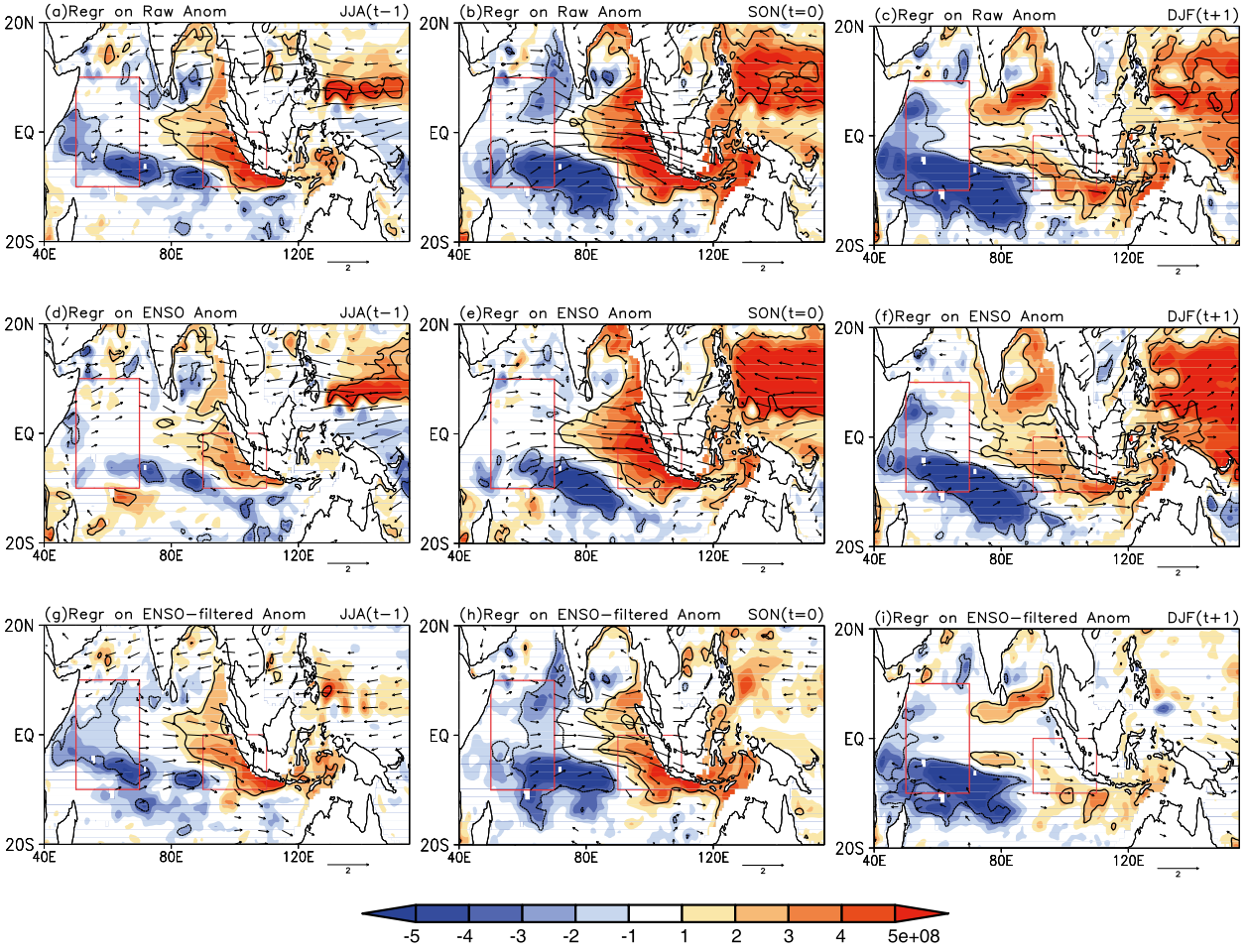

FIG. 4. Fall-centered seasonal lead–lag regressions of three versions of the E-IOD SST index on upper-ocean (0–381 m) heat content (OHC, from SODA 2.1.6 ocean reanalysis) and 850-hPa winds (from ERA-40 atmospheric reanalysis): shown are regressions of the (top) "raw" (i.e., unfiltered) index, (middle) an index constructed from just ENSO-related IO variability, and (bottom) the ENSO-filtered E-IOD index. Note that the index and regressions are obtained from the same dataset in all cases. The (left) summer (JJA) anomalies are the one-season lead regressions while the (right) winter (DJF) ones are the 1-season lag regressions; (middle) contemporaneous (fall, SON) ones are in the middle column. The OHC regressions are shaded/contoured in warm (positive) and cool (negative) colors with an interval/threshold of 10^8 J m^{-2}: see color bar. Wind vector scales are shown below each panel. All datasets were detrended (following footnote 1) and the zero contour is omitted in all panels. Regressions significant at the 0.05 level are contoured in black.

implicated in regional drought over eastern Africa (Saji et al. 1999; Goddard and Graham 1999; Latif et al. 1999).

The top row shows the E-IOD linked OHC anomalies in the eastern IO to peak in fall but anomalies in the southwestern equatorial IO basin attain maximum amplitude in boreal winter. The precursor (JJA) near-surface wind anomalies include easterlies over peninsular India, which weaken the climatological monsoonal flow (southwesterly), leading to diminished summer monsoon rainfall. Regardless of the season, OHC anomalies in the western basin are seldom focused in the W-IOD box (marked).

The strong westerly anomalies over the tropical IO basin and stronger easterlies over the north-equatorial Pacific are part of a larger east–west atmospheric circulation anomaly centered over the Maritime Continent, as apparent from more expansive plots (not shown). The larger-scale anomaly structure is indicative of ENSO's influence, which is analyzed by computing both the E-IOD index and its regressions from just the ENSO signal over the IO basin (Figs. 4d–f); extraction of the full ENSO signal was discussed earlier. That the ENSO signal dominates the regressions of the raw E-IOD index is evident from the striking similarity of the top two rows. ENSO's impressive influence on the IO is, of course, transmitted through its impact on surface winds over the IO basin (e.g., Nigam and Shen 1993; Xie et al. 2002). Regardless, the case for filtering the externally generated ENSO influence from IO variability prior to an objective search for recurrent variability

TABLE 1. Sensitivity analysis: T0 is the primary analysis, which was perturbed as listed below to assess robustness of the extracted variability modes. In all cases, SST was detrended using the nonstationary SST secular trend mode (see footnote 1), and is called ''DeTrend'' here. A zero in the ''Rotated'' column indicates that loading vectors were not rotated.

Name	Domain	Period	Rotated	Sampling window	SST
T0	Indian Ocean	1902–2007	2	7-season	DeTrend, Pacific basin influence
T1	Indian Ocean	1902–2007	0	7-season	DeTrend, Pacific basin influence
T2	Indian Ocean	1902–2007	3	7-season	DeTrend, Pacific basin influence
T3	Indian Ocean	1902–2007	0	5-season	DeTrend, Pacific basin influence
T4	Indian Ocean	1902–2007	0	7-season	DeTrend, Pacific and Atlantic basin influences
T5	Indian Ocean	1902–2007	0	7-season	DeTrend

structures across this basin is reinforced by the above analysis.

Finally, the structure of internally generated variability in the IO basin is revealed in Figs. 4g–i (bottom row) via regressions of the E-IOD index; the index and regressions are both obtained from ENSO-filtered IO variability. Not unexpectedly, OHC anomalies are now present primarily in the IO basin. But, somewhat surprisingly, a coherent dipole structure is manifest, with the western basin anomalies somewhat better positioned vis-à-vis the W-IOD box. The analysis supports the finding of the previous section, namely that internally generated variability in the tropical IO basin can exhibit a zonal-dipole structure at the subsurface.

6. Recurrent modes of variability in filtered Indian Ocean SSTs

An objective search for the recurrent modes of variability of Indian Ocean SSTs is undertaken, in contrast to the analysis of variability patterns in the preceding sections. The distinction between mode and pattern is important as the former refers to a unique spatiotemporal variability structure while the latter to just a spatial pattern of variability that is linked, potentially, with more than one time scale. Another difference is that previous analyses factored for just ENSO's influence on the IO basin, while the present one will also factor for the influence of Pacific decadal SST variability. Finally, the previous sections were too focused on the E-IOD because it was the more viable of the IOD poles, but it is unclear if the E-IOD region would emerge as a key variability center in an objective analysis of filtered IO SSTs.

a. SST filtering

Recurrent spatiotemporal structure of SST variability in the Indian Ocean is analyzed after filtering the influence of both interannual and decadal Pacific SST variability. The influence of ENSO variability was estimated in section 3; the impact of decadal variability is, likewise, estimated from regressions of the pan-Pacific and North Pacific PCs (GN2008). The first mode, with a horseshoe structure in the Pacific, exhibits connections to the tropical–subtropical Atlantic resembling the AMO. The second, capturing the 1976/77 climate shift, is similar to Pacific decadal oscillation (Mantua et al. 1997) in structure but with interesting links to the IO SSTs (cf. Fig. 12 in GN2008). The SST record was already detrended earlier using regressions of the nonstationary SST secular trend (cf. footnote 1); this mode captures the widespread but nonuniform warming of all basins along with a sliver of cooling in the central equatorial Pacific.[4]

b. Analysis technique

The filtered, seasonal SST anomalies during 1902–2007 were analyzed in the Indian Ocean basin (40°S–30°N, 20°–120°E) using the extended-EOF technique (Weare and Nasstrom 1982); seven-season-long anomaly sequences were targeted in the primary analysis (T0) where two leading loading vectors are rotated. Robustness of the variability modes was ascertained by perturbing the primary analysis: no rotation of loading vectors (T1), rotation of three loading vectors (T2), shorter (five season long) sampling window (T3), Indian Ocean SSTs additionally filtered for Atlantic's influence (T4), and Indian Ocean SSTs are only detrended but not filtered for any external influences (T5); all are listed in Table 1.

Table 2 describes the sensitivity analysis results, including temporal correlation of the PCs of the primary and perturbed analyses. An observational realization of the mode is the ultimate proof of its physicality. But it is seldom that observed anomalies are composed of just one mode of variability (i.e., with all other modes suppressed at that time); of course, should this happen, an observational ''analog'' of that mode is encountered. The number of observational analogs of an extracted set

[4] The physicality of the decadal modes was evaluated using analog counts and fish recruitment records in GN2008.

TABLE 2. Sensitivity results: Column 1 shows the leading modes identified in the primary analysis (T0); numbers following the name indicate the percentage variance explained by the mode and its rank, respectively. Columns 2–6 list attributes of the leading modes in the five sensitivity tests (T1–T5), with the three-slash numbers indicating correlation between the test case and primary analysis PC, the percentage variance explained by that mode, and its rank in the test analysis. Asterisks indicate ''no match.'' All correlation coefficients are significant at the 0.001 level.

T0	T1	T2	T3	T4	T5
IND1/10.9/1	0.96/11.4/1	0.98/10.3/1	0.94/12.6/1	0.92/10.9/1	0.67/6.7/3
IND2/5.5/2	0.96/5.0/2	0.82/5.1/3	0.88/6.3/2	0.71/5.2/2	*

of modes in the anomaly record is one objective measure of the ''physicality'' of that extraction, and the primary analysis is chosen in this manner. An observed anomaly will be deemed a modal analog if any one PC is larger than all others in that analysis by at least one unit of magnitude; note that PCs are orthonormal with or without rotation. The identification is objective and easily implemented, and Table 3 lists the number of analogs in the six analyses (T0–T5): Considering just the first two PCs, 128 seasonal anomalies (out of the 424 analyzed) are found to be analogs of the first or second mode in the T0 analysis.

c. *Analysis results*

The two leading PCs from the primary analysis (T0) are shown in Fig. 5a. The leading PC accounts for ~11% of the variance, and represents subdecadal variability with a notable warm phase in the 1970s–1980s. As seen later (Fig. 6), the represented SST variability has a meridional dipole structure with a pronounced southern pole in the subtropical Southern Hemisphere (SH) basin (focused southward of Mauritius); this region was anomalously warm during the 1970s to 1980s. The second PC (explaining 5%–6% of variance) represents, principally, interannual variability; the related loading vector (Fig. 6) is more tropically focused and resembles the IOD structure in the western-central basin; the similarity with IOD ends here, however, as shown and discussed later. Unlike the leading mode, this one exhibits considerable structural evolution, evolving into a meridional dipole (with a stronger northern pole) in the SH tropical–subtropical basin before dissipating (Fig. 6). Potential links with the IOD and the subtropical IOD (SIOD; Behera and Yamagata 2001) are investigated in Figs. 5b and 6.

The autocorrelation structure of the PCs is examined in Fig. 5b to estimate the modal time scale; a conservative estimate follows from the temporal distance of points where autocorrelation is e^{-1} (≈0.37), yielding ~6 years for PC1 and 2–3 years for PC2. The autocorrelation structure of the IOD and SIOD indices is also displayed in Fig. 5b, for context; both, evidently, represent much shorter time scale (~1 yr) variability. The correlation of PC1 and the IOD (SIOD) index is 0.14 (0.47), significant at the 0.001 level. The corresponding PC2 correlations are −0.11 and 0.22, at the 0.05 significance level. The IOD is thus unrelated to the extracted modes which exhibit some pattern (but not time scale) similarity to SIOD variability.

Spatiotemporal evolution of the SST variability modes in the T0 analysis is displayed in the first two columns of Fig. 6. Seasonal lead–lag regressions of the fall-season (SON) PCs are shown in order to compare with the IOD pattern (third column), which is robust in fall; the fourth column depicts evolution of the subtropical IOD using its winter (DJF)-based index. The five-season evolution (time running downward) clearly conveys the variability time scales: significantly longer than five seasons for PC1, just about this period for PC2, and shorter than five seasons for both IOD and SIOD, consistent with the autocorrelation analysis (Fig. 5b).

The evolution of the leading mode is not seasonally sensitive in view of its ~6-yr time scale but others are, as manifest from the regressions centered on other seasons (not shown). As noted earlier, the leading mode is focused in the SH with large amplitudes in the western subtropics. The second mode, in contrast, has footprints in the northern basin as well, and shows significant spatiotemporal development: evolving from a single-signed anomaly pattern in the tropics in spring–fall into a meridional dipole in the SH subtropics in boreal winter (DJF); note the similarity of the winter patterns in the SH.[5] The second mode dissipates by the following spring [March–May (MAM)] whereas the first mode shows no such sign.

A comparison of columns 2 and 3 indicates both similarities and differences between the second mode of this analysis and the IOD. Key differences include the lack of modal amplitude in the western basin (including Arabian Sea) in fall (SON) and the absence of a zonal-dipole structure in the tropics (e.g., no modal amplitude off Sumatra). The similarity accrues from the amplitude focus in the central basin in boreal fall–winter (SON,

[5] An extended-EOF analysis is well positioned to distinguish variability structures having similar spatial footprint but different time scales and evolution.

TABLE 3. Analog counts: Number of "analogs" in six extended-EOF analyses of Indian Ocean SST variability during 1902–2007. An analog is identified when the absolute value of the PC of any one mode is larger than that of *all* others by at least one unit; note PCs are orthonormal. Mathematically, if $||PC_i| - |PC_j|| > 1.00$ for all j not equal to i, an analog is counted. For consistent evaluation, only analogs of the two leading modes are counted.

T0	T1	T2	T3	T4	T5
128	96	87	98	97	95

DJF), especially structure in the SH tropics (e.g., northwest-to-southeast amplitude tilt). The regression patterns are most similar in boreal winter (DJF) when both exhibit some resemblance with the subtropical IOD pattern in the SH.

The analysis indicates that the SH subtropical Indian Ocean exhibits SIOD-type variability patterns, but on both decadal and interannual time scales. The interannual one undergoes significant metamorphosis, beginning with single-signed anomalies in the tropics and ending in a SIOD-type structure in boreal winter (DJF).

d. Link with continental precipitation

Precipitation links of the IO SST variability modes are shown in Fig. 7, beginning with boreal summer (JJA, top panels); contemporaneous correlations are shown to gauge significance of the links. PC-1, representing subdecadal SST variability in the subtropical SH basin, is linked with diminished summer rainfall over sub-Saharan Africa (including the Sahel). The links are weak elsewhere except Southeast Asia where correlations are significantly positive. During boreal fall (SON), PC1 continues to be linked with rainfall deficits over the western-central Sahel, but positive links emerge over the Congo basin and to its southeast; rainfall variability in these regions has been linked to higher SST in the southwestern Indian Ocean (Behera and Yamagata 2001; Xie and Arkin 1996; Reason 2001). In austral summer (DJF), PC1 is positively linked with increased rainfall in northern–central Australia; the correlation distribution suggests a southward excursion of the monsoon rainfall belt.

Precipitation links of the interannual SST mode (PC2) are generally weaker (Fig. 7, right column). The links have some structure in fall (SON) when Sahel is wetter and eastern equatorial Africa marginally drier; southeastern Australia is wetter during this time (austral spring).

7. Concluding remarks

The viability of the Indian Ocean dipole (IOD) mode of SST variability is investigated almost a dozen years after it was proposed (Saji et al. 1999), and just about

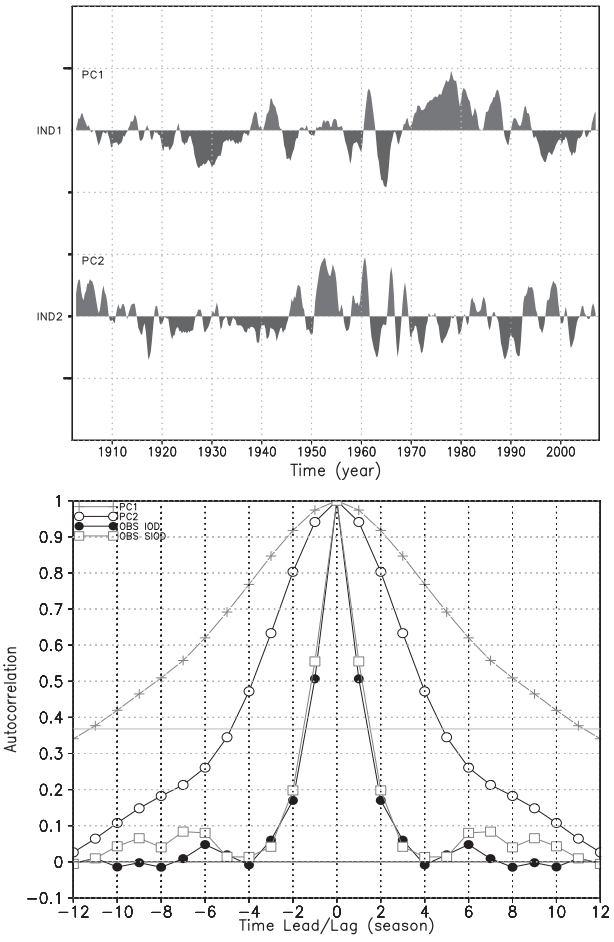

FIG. 5. (top) Principal components (PCs) of the two leading modes of recurrent spatiotemporal SST variability in the Indian Ocean. The PCs are obtained from rotated, extended-EOF analysis of Pacific-uninfluenced, nonseasonal Indian Ocean SST variability during 1902–2007; PC1 and PC2 explain 10.9% and 5.5% of the variance, respectively. Tick marks on the vertical axis are drawn every three standard deviations. (bottom) The autocorrelation structure of the two PCs and the IOD and subtropical IOD (SIOD) indices.

a decade after intense discussion of its physicality (Allan et al. 2001; Dommenget and Latif 2002; Hastenrath 2002; Behera et al. 2003; Yamagata et al. 2003; and others). At times, the discussion became lively, as with Philander's (2003) metaphoric use of a cow for IOD's complex structure. Given the close scrutiny, especially of IOD's relationship with ENSO in these critiques and follow-on studies, there is some obligation to state the reasons for revisiting this issue.

Our primary interest, in fact, was assessment of the impact of Indian Ocean (IO) SSTs on Chinese summer rainfall, as part of a broader effort to understand the reasons for the drying of northern China in recent decades. Toward this end, we investigated the structure of

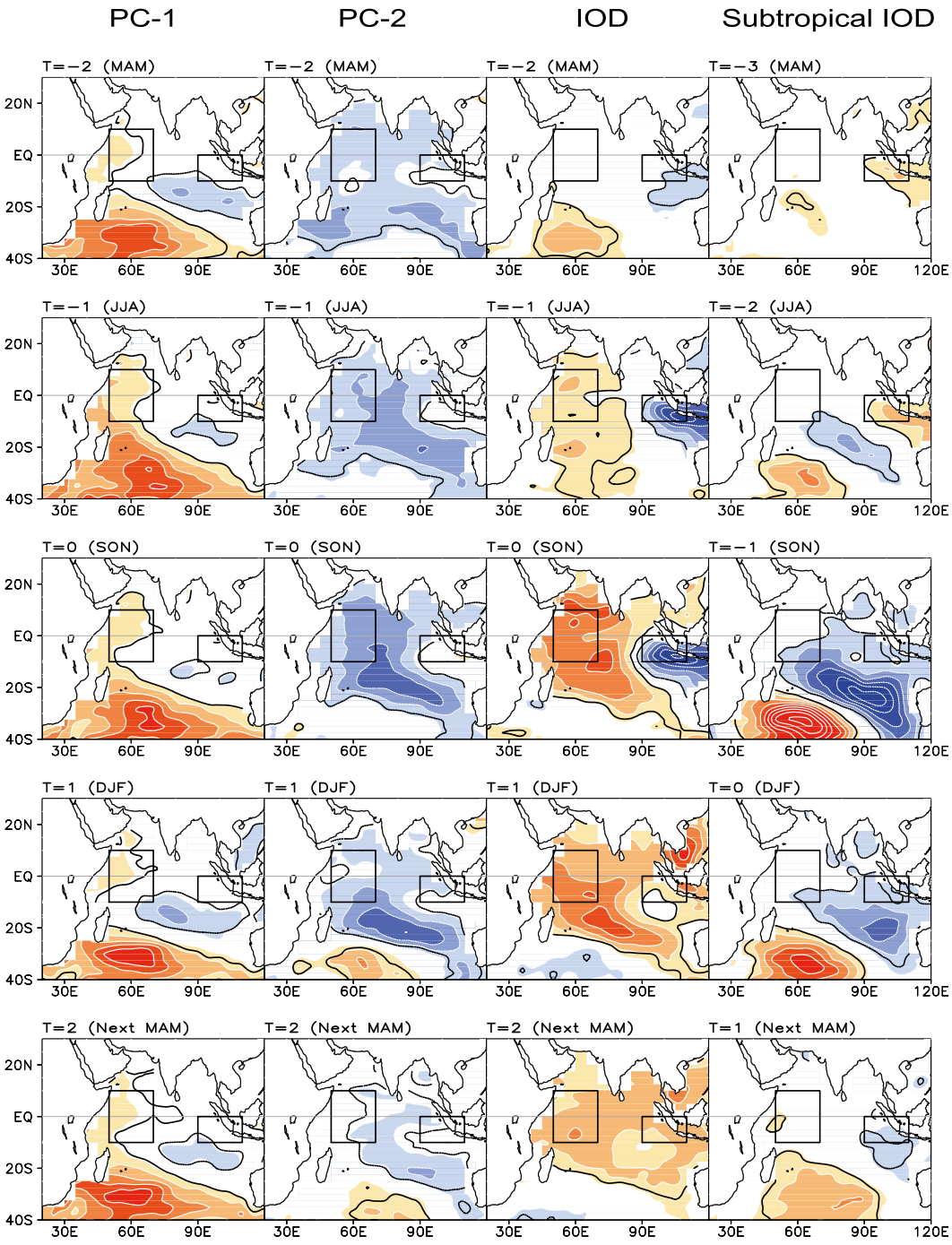

FIG. 6. Spatiotemporal evolution of recurrent SST variability in the Indian Ocean: Seasonal lead–lag regressions of the leading principal components (PC1 and PC2) are shown in the left two columns, with time increasing downward. Fall-centered regressions (i.e., of the fall PC values) are shown to facilitate comparison with the IOD structure which is robust in boreal fall (SON). Indian Ocean SSTs are filtered for the Pacific's influence (as in T0 analysis) prior to computation of regressions. *Fall*-centered regressions of the IOD and *winter*-centered (DJF) regressions of the subtropical IOD on unfiltered Indian Ocean SSTs are shown in the far right columns. The western and eastern IOD box is displayed in all panels to facilitate IOD recognition. Regressions are for the 1902–2007 period, and detrended SSTs are the starting point in all cases. Contour interval and shading threshold is 0.05 K, and positive values are shown in warm colors; zero-contour is omitted in all panels. Regressions significant at the 0.05 level are contoured in black.

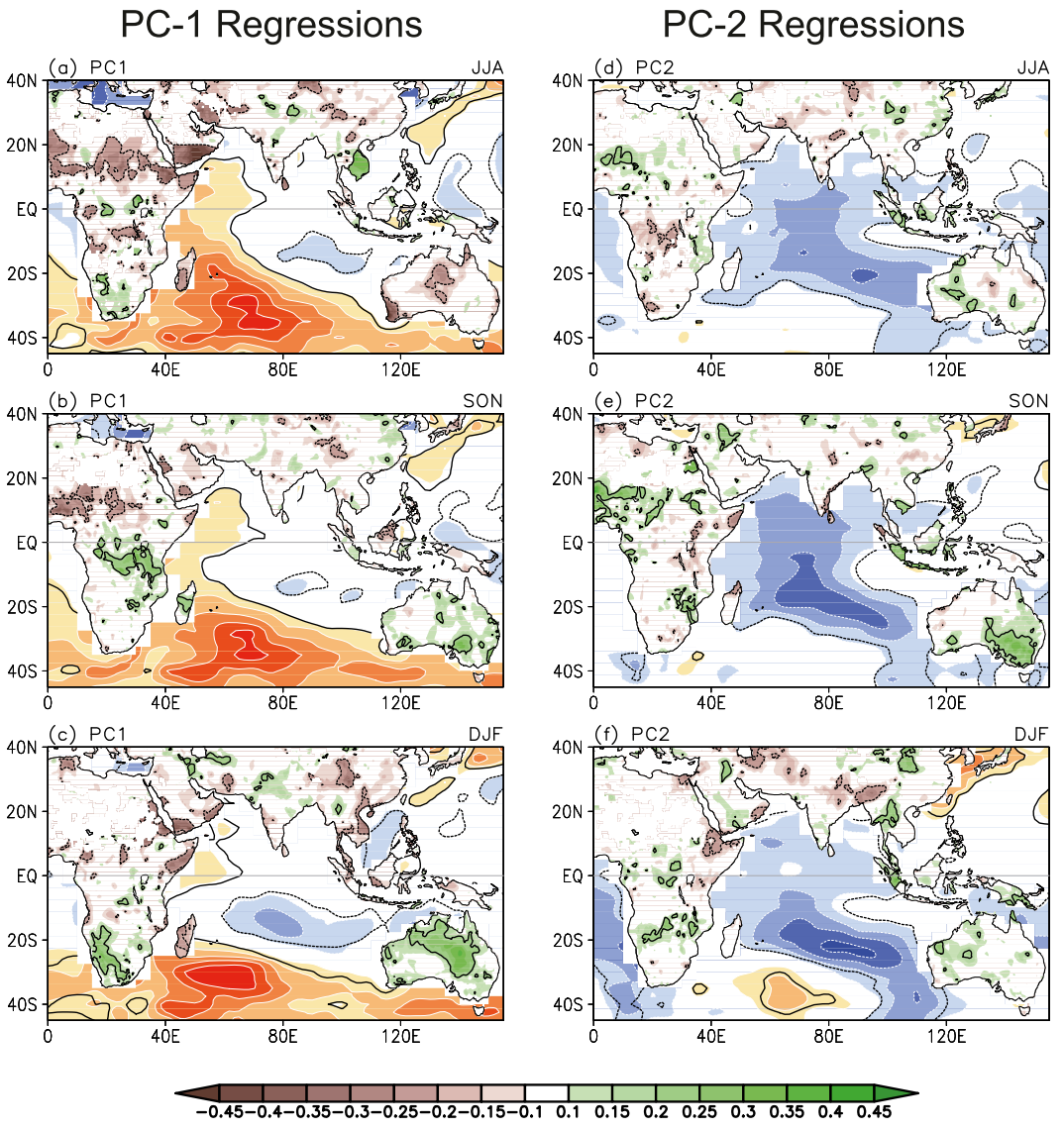

FIG. 7. Seasonal regressions/correlations of the Indian Ocean SST principal components on the Pacific-uninfluenced Indian Ocean SST and adjoining continental precipitation: (top) JJA, (middle) SON, and (bottom) DJF. SST regressions are shaded and contoured in warm (positive) and cool (negative) colors with an interval/threshold of 0.05K. Correlations with CRU TS3.1's half-degree continental precipitation are shown with a shading threshold of 0.10 and an interval of 0.05; see color bar. All data sets were detrended (following footnote 1) and the zero contour is omitted in all panels. Regressions/correlations significant at the 0.05 level are contoured in black.

recurrent spatiotemporal variability of IO SSTs in the twentieth century, factoring for Pacific SSTs' influence (including ENSO). To our surprise, the IOD was not among the extracted modes in our surface (SST) analysis, piquing our interest in Saji et al.'s study.

Interestingly, it is neither new observational data nor deployment of refined analysis techniques or improved climate models that lead to the finding that IOD is, in part, an artifact of ENSO's influence on the IO basin. The zonal-dipole SST structure—the defining IOD attribute—crumbles when ENSO's influence on IO SSTs is removed *prior* to any analysis of IO SST variability. Saji et al. (1999) took their leading, seasonally invariant SST EOF, with monopolar structure in the IO basin, to be ENSO's *entire* influence,[6] and proceeded to define the dipole mode index (DMI) on

[6] This too would not be different from the physicist representing the cow as a sphere in Philander's brief perspective on the IOD–ENSO debate titled "Of dipoles and spherical cows" (Philander 2003).

the basis of the second EOF's structure. As the EOFs are temporally orthogonal, Saji et al. viewed the IOD (based on DMI) to be ENSO-independent. ENSO's full influence on IO SSTs was, of course, not captured by Saji et al.'s first mode. Although capturing ENSO's full influence is nontrivial, as discussed in GN2008 and Compo and Sardeshmukh (2010), and earlier in section 3 and 6a of this study, we show that a zonal-dipole variability structure is untenable even when a rudimentary estimate of ENSO's influence on IO SSTs (from Niño-3.4 SST index regressions) is filtered in advance of IO SST variability analysis.

Not surprisingly, Dommenget (2011) reached a similar conclusion, namely that variations of the IO zonal SST gradient (or DMI) are not independent of ENSO, using the distinct EOF (DEOF) analysis technique (Dommenget 2007) where a first-order autoregressive model is used to generate the null hypothesis for the EOF patterns. This analysis, like ours, revealed no coherent connection between the two DMI centers at the surface. Meyers et al. (2007) also sought to remove the ENSO signal from the IO SSTs prior to the IO analysis, using a lagged-EOF technique that seeks to capture a spatiotemporally evolving signal (e.g., ENSO) as a single mode. The efficacy of this technique in capturing ENSO's complex variability, however, was not assessed by the authors (e.g., from correlations of the observed and reconstructed Niño-3.4 SST indices). The method involves restoring phase lags—a daunting task when the variability mode exhibits multiple time scales, not all of which are a priori known. Some differences in assessment of the IOD–ENSO relationship among analyses are thus expected. Note that our extended-EOF analysis (Weare and Nasstrom 1982) is equivalent to the widely used multichannel singular spectrum analysis (von Storch and Zwiers 1999).

Unable to find a zonal-dipole mode of *internal* variability at the surface (SST), we extended the search to the subsurface realm, specifically upper-ocean (0–381 m) heat content (OHC) variations. The search was first conducted in context of the two recent fall-period IO SST anomalies (1994 and 1997), both of which are classified as positive IOD events (e.g., Saji et al. 1999), with a DMI index of +0.60 and +1.05, respectively. Deconstruction of the fall SST anomalies revealed a DMI index of +0.25 and −0.09 in the ENSO-filtered SST anomalies (i.e., a weak IOD event in 1994 and none at all in 1997). Deconstruction of the OHC anomalies did indicate a zonal-dipole structure in 1994 but with the western pole positioned to the right of the western IOD box; no dipole was manifest in 1997 in the ENSO-filtered OHC. This limited analysis suggests that internally generated variability in the tropical IO basin can exhibit zonal-dipole structure, but perhaps only at the subsurface. This finding, based on two cases, was corroborated from regressions of the E-IOD index (based on SST anomalies in the eastern IOD box) on OHC over a 40-yr period.

Finally, we report on an objective search for the recurrent *modes* of variability of IO SSTs from which the influence of both ENSO and Pacific decadal SST variability has been removed. The reported search for the internally generated modes of IO variability is different from prior analyses that typically focus on recurrent spatial patterns, in contrast with spatiotemporal patterns in the present search. Interestingly, none of the extracted modes was found to exhibit a zonal-dipole structure in SST. The second leading mode does have a dipole-like structure but in the meridional direction and in boreal fall/winter, when it resembles the subtropical IOD (SIOD) pattern. The resemblance, however, stops there as this mode's evolution time scale is considerably longer than the SIOD's. The seasonally evolving continental precipitation links of the two SST variability modes contain interesting features over sub-Saharan Africa, the Congo basin, and northern-central Australia.

Our study calls into question the edifice built on the DMI index, including constructs such as the Equatorial Indian Ocean Oscillation (EQUINOO)–(IOD-related zonal surface wind variability at the equator (Gadgil et al. 2004).

Acknowledgments. The authors thank Bin Guan (NASA/JPL) and Alfredo Ruiz-Barradas (University of Maryland) for advice and technical help with data analysis. This work is part of the doctoral dissertation of the first author.

REFERENCES

Allan, R. J., and Coauthors, 2001: Is there an Indian Ocean dipole and is it independent of the El Niño–Southern Oscillation? *CLIVAR Exchanges,* No. 6, International CLIVAR Project Office, Southampton, United Kingdom, 18–22.

Ashok, K., Z. Y. Guan, and T. Yamagata, 2003: A look at the relationship between the ENSO and the Indian Ocean dipole. *J. Meteor. Soc. Japan,* **81,** 41–56, doi:10.2151/jmsj.81.41.

——, S. K. Behera, S. A. Rao, H. Y. Weng, and T. Yamagata, 2007: El Niño Modoki and its possible teleconnection. *J. Geophys. Res.,* **112,** C11007, doi:10.1029/2006JC003798.

Baquero-Bernal, A., M. Latif, and S. Legutke, 2002: On dipolelike variability of sea surface temperature in the tropical Indian Ocean. *J. Climate,* **15,** 1358–1368, doi:10.1175/1520-0442(2002)015<1358:ODVOSS>2.0.CO;2.

Behera, S. K., and T. Yamagata, 2001: Subtropical SST dipole events in the southern Indian Ocean. *Geophys. Res. Lett.,* **28,** 327–330, doi:10.1029/2000GL011451.

——, R. Krishnan, and T. Yamagata, 1999: Unusual ocean–atmosphere conditions in the tropical Indian Ocean during

1994. *Geophys. Res. Lett.,* **26,** 3001–3004, doi:10.1029/1999GL010434.

——, S. A. Rao, H. N. Saji, and T. Yamagata, 2003: Comments on ''A cautionary note on the interpretation of EOFs''. *J. Climate,* **16,** 1087–1093, doi:10.1175/1520-0442(2003)016<1087:COACNO>2.0.CO;2.

——, J. J. Luo, S. Masson, S. A. Rao, H. Sakuma, and T. Yamagata, 2006: A CGCM study on the interaction between IOD and ENSO. *J. Climate,* **19,** 1688–1705, doi:10.1175/JCLI3797.1.

Carton, J. A., and B. S. Giese, 2008: A reanalysis of ocean climate using Simple Ocean Data Assimilation (SODA). *Mon. Wea. Rev.,* **136,** 2999–3017, doi:10.1175/2007MWR1978.1.

——, G. Chepurin, and X. Cao, 2000: A Simple Ocean Data Assimilation analysis of the global upper ocean 1950–95. Part II: Results. *J. Phys. Oceanogr.,* **30,** 311–326, doi:10.1175/1520-0485(2000)030<0311:ASODAA>2.0.CO;2.

Chambers, D., B. Tapley, and R. Stewart, 1999: Anomalous warming in the Indian Ocean coincident with El Niño. *J. Geophys. Res.,* **104,** 3035–3047, doi:10.1029/1998JC900085.

Clarke, A. J., and X. Liu, 1993: Observations and dynamics of semiannual and annual sea levels near the eastern equatorial Indian Ocean boundary. *J. Phys. Oceanogr.,* **23,** 386–399, doi:10.1175/1520-0485(1993)023<0386:OADOSA>2.0.CO;2.

Compo, G. P., and P. D. Sardeshmukh, 2010: Removing ENSO-related variations from the climate record. *J. Climate,* **23,** 1957–1978, doi:10.1175/2009JCLI2735.1.

Dommenget, D., 2007: Evaluating EOF modes against a stochastic null hypothesis. *Climate Dyn.,* **28,** 517–531, doi:10.1007/s00382-006-0195-8.

——, 2011: An objective analysis of the observed spatial structure of the tropical Indian Ocean SST variability. *Climate Dyn.,* **36,** 2129–2145, doi:10.1007/s00382-010-0787-1.

——, and M. Latif, 2002: A cautionary note on the interpretation of EOFs. *J. Climate,* **15,** 216–225, doi:10.1175/1520-0442(2002)015<0216:ACNOTI>2.0.CO;2.

——, V. Semenov, and M. Latif, 2006: Impacts of the tropical Indian and Atlantic Oceans on ENSO. *Geophys. Res. Lett.,* **33,** L11701, doi:10.1029/2006GL025871.

Frauen, C., and D. Dommenget, 2012: Influences of the tropical Indian and Atlantic Oceans on the predictability of ENSO. *Geophys. Res. Lett.,* **39,** L02706, doi:10.1029/2011GL050520.

Gadgil, S., P. Vinayachandran, P. Francis, and S. Gadgil, 2004: Extremes of the Indian summer monsoon rainfall, ENSO and equatorial Indian Ocean oscillation. *Geophys. Res. Lett.,* **31,** L12213, doi:10.1029/2004GL019733.

Goddard, L., and N. E. Graham, 1999: Importance of the Indian Ocean for simulating rainfall anomalies over eastern and southern Africa. *J. Geophys. Res.,* **104,** 19 099–19 116, doi:10.1029/1999JD900326.

Guan, B., and S. Nigam, 2008: Pacific sea surface temperatures in the twentieth century: An evolution-centric analysis of variability and trend. *J. Climate,* **21,** 2790–2809, doi:10.1175/2007JCLI2076.1.

——, and ——, 2009: Analysis of Atlantic SST variability factoring interbasin links and the secular trend: Clarified structure of the Atlantic multidecadal oscillation. *J. Climate,* **22,** 4228–4240, doi:10.1175/2009JCLI2921.1.

Hastenrath, S., 2002: Dipoles, temperature gradient, and tropical climate anomalies. *Bull. Amer. Meteor. Soc.,* **83,** 735–738, doi:10.1175/1520-0477(2002)083<0735:WLACNM>2.3.CO;2.

Horii, T., H. Hase, I. Ueki, and Y. Masumoto, 2008: Oceanic precondition and evolution of the 2006 Indian Ocean dipole. *Geophys. Res. Lett.,* **35,** L03607, doi:10.1029/2007GL032464.

Huang, B., and J. Shukla, 2007a: Mechanisms for the interannual variability in the tropical Indian Ocean. Part I: The role of remote forcing from the tropical Pacific. *J. Climate,* **20,** 2917–2936, doi:10.1175/JCLI4151.1.

——, and ——, 2007b: Mechanisms for the interannual variability in the tropical Indian Ocean. Part II: Regional processes. *J. Climate,* **20,** 2937–2960, doi:10.1175/JCLI4169.1.

Izumo, T., and Coauthors, 2010: Influence of the state of the Indian Ocean dipole on the following year's El Niño. *Nat. Geosci.,* **3,** 168–172, doi:10.1038/ngeo760.

Jansen, M. F., D. Dommenget, and N. Keenlyside, 2009: Tropical atmosphere–ocean interactions in a conceptual framework. *J. Climate,* **22,** 550–567, doi:10.1175/2008JCLI2243.1.

Kug, J.-S., and I.-S. Kang, 2006: Interactive feedback between ENSO and the Indian Ocean. *J. Climate,* **19,** 1784–1801, doi:10.1175/JCLI3660.1.

Latif, M., D. Dommenget, M. Dima, and A. Grötzner, 1999: The role of Indian Ocean sea surface temperature in forcing East African rainfall anomalies during December–January 1997/98. *J. Climate,* **12,** 3497–3504, doi:10.1175/1520-0442(1999)012<3497:TROIOS>2.0.CO;2.

Luo, J. J., S. Behera, Y. Masumoto, H. Sakuma, and T. Yamagata, 2008: Successful prediction of the consecutive IOD in 2006 and 2007. *Geophys. Res. Lett.,* **35,** L14S02, doi:10.1029/2007GL032793.

——, R. Zhang, S. K. Behera, Y. Masumoto, F.-F. Jin, R. Lukas, and T. Yamagata, 2010: Interaction between El Niño and extreme Indian Ocean dipole. *J. Climate,* **23,** 726–742, doi:10.1175/2009JCLI3104.1.

Mantua, N. J., S. R. Hare, Y. Zhang, J. M. Wallace, and R. C. Francis, 1997: A Pacific interdecadal climate oscillation with impacts on salmon production. *Bull. Amer. Meteor. Soc.,* **78,** 1069–1079, doi:10.1175/1520-0477(1997)078<1069:APICOW>2.0.CO;2.

Meehl, G. A., J. M. Arblaster, and J. Loschnigg, 2003: Coupled ocean–atmosphere dynamical processes in the tropical Indian and Pacific Oceans and the TBO. *J. Climate,* **16,** 2138–2158, doi:10.1175/2767.1.

Merle, J., 1980: Seasonal heat budget in the equatorial Atlantic Ocean. *J. Phys. Oceanogr.,* **10,** 464–469, doi:10.1175/1520-0485(1980)010<0464:SHBITE>2.0.CO;2.

Meyers, G., P. McIntosh, L. Pigot, and M. Pook, 2007: The years of El Niño, La Niña, and interactions with the tropical Indian Ocean. *J. Climate,* **20,** 2872–2880, doi:10.1175/JCLI4152.1.

Murtugudde, R., J. P. McCreary, and A. J. Busalacchi, 2000: Oceanic processes associated with anomalous events in the Indian Ocean with relevance to 1997–1998. *J. Geophys. Res.,* **105,** 3295–3306, doi:10.1029/1999JC900294.

Nicholls, N., and W. Drosdowsky, 2001: Is there an equatorial Indian Ocean SST dipole, independent of the El Niño Southern Oscillation? Preprints, *Conf. on Climate Variability, the Oceans, and Societal Impacts,* Albuquerque, New Mexico, Amer. Meteor. Soc., 1.9 [Available online at https://ams.confex.com/ams/annual2001/techprogram/paper_17337.htm.]

Nigam, S., and H.-S. Shen, 1993: Structure of oceanic and atmospheric low-frequency variability over the tropical Pacific and Indian Oceans. Part I: COADS observations. *J. Climate,* **6,** 657–676, doi:10.1175/1520-0442(1993)006<0657:SOOAAL>2.0.CO;2.

Philander, S. G., 2003: Of dipoles and spherical cows. *Bull. Amer. Meteor. Soc.,* **84,** 1424, doi:10.1175/BAMS-84-10-1424Philander.

Rasmusson, E. M., X. Wang, and C. F. Ropelewski, 1990: The biennial component of ENSO variability. *J. Mar. Syst.,* **1,** 71–96, doi:10.1016/0924-7963(90)90153-2.

Rayner, N. A., D. E. Parker, E. B. Horton, C. K. Folland, L. V. Alexander, D. P. Rowell, E. C. Kent, and A. Kaplan, 2003: Global analyses of sea surface temperature, sea ice, and night marine air temperature since the late nineteenth century. *J. Geophys. Res.,* **108,** 4407, doi:10.1029/2002JD002670.

Reason, C., 2001: Subtropical Indian Ocean SST dipole events and southern African rainfall. *Geophys. Res. Lett.,* **28,** 2225–2227, doi:10.1029/2000GL012735.

——, R. Allan, J. Lindesay, and T. Ansell, 2000: ENSO and climatic signals across the Indian Ocean basin in the global context. Part I: Interannual composite patterns. *Int. J. Climatol.,* **20,** 1285–1327, doi:10.1002/1097-0088(200009)20:11<1285::AID-JOC536>3.0.CO;2-R.

Saji, N. H., B. N. Goswami, P. N. Vinayachandran, and T. Yamagata, 1999: A dipole mode in the tropical Indian Ocean. *Nature,* **401,** 360–363.

Shinoda, T., H. H. Hendon, and M. A. Alexander, 2004: Surface and subsurface dipole variability in the Indian Ocean and its relation with ENSO. *Deep Sea Res.,* **51,** 619–635, doi:10.1016/j.dsr.2004.01.005.

Uppala, S. M., and Coauthors, 2005: The ERA-40 Re-Analysis. *Quart. J. Roy. Meteor. Soc.,* **131,** 2961–3012, doi:10.1256/qj.04.176.

von Storch, H., and F. W. Zwiers, 1999: *Statistical Analysis in Climate Research.* Cambridge University Press, 484 pp.

Weare, B. C., and J. S. Nasstrom, 1982: Examples of extended empirical orthogonal function analyses. *Mon. Wea. Rev.,* **110,** 481–485, doi:10.1175/1520-0493(1982)110<0481:EOEEOF>2.0.CO;2.

Webster, P. J., A. M. Moore, J. P. Loschnigg, and R. R. Leben, 1999: Coupled ocean–atmosphere dynamics in the Indian Ocean during 1997–98. *Nature,* **401,** 356–360, doi:10.1038/43848.

Wu, R., and B. P. Kirtman, 2004: Understanding the impacts of the Indian Ocean on ENSO variability in a coupled GCM. *J. Climate,* **17,** 4019–4031, doi:10.1175/1520-0442(2004)017<4019:UTIOTI>2.0.CO;2.

Wyrtki, K., 1973: Physical oceanography of the Indian Ocean. *The Biology of the Indian Ocean,* Springer, 18–36.

Xie, P., and P. A. Arkin, 1996: Analyses of global monthly precipitation using gauge observations, satellite estimates, and numerical model predictions. *J. Climate,* **9,** 840–858, doi:10.1175/1520-0442(1996)009<0840:AOGMPU>2.0.CO;2.

Xie, S.-P., H. Annamalai, F. A. Schott, and J. P. McCreary, 2002: Structure and mechanisms of south Indian Ocean climate variability. *J. Climate,* **15,** 864–878, doi:10.1175/1520-0442(2002)015<0864:SAMOSI>2.0.CO;2.

Yamagata, T., S. K. Behera, S. A. Rao, Z. Guan, K. Ashok, and H. N. Saji, 2003: Comments on ''Dipoles, temperature gradients, and tropical climate anomalies.'' *Bull. Amer. Meteor. Soc.,* **84,** 1418–1422, doi:10.1175/BAMS-84-10-1418.

——, ——, J. J. Luo, S. Masson, M. R. Jury, and S. A. Rao, 2004: Coupled ocean–atmosphere variability in the tropical Indian Ocean. *Ocean–Atmosphere Interaction and Climate Variability, Geophys. Monogr.,* Vol. 147, Amer. Geophys. Union, 189–212.

Yu, J.-Y., and K. M. Lau, 2005: Contrasting Indian Ocean SST variability with and without ENSO influence: A coupled atmosphere–ocean GCM study. *Meteor. Atmos. Phys.,* **90,** 179–191, doi:10.1007/s00703-004-0094-7.